J Mater Sci: Mater Med (2007) 18:9–23
DOI 10.1007/s10856-006-0658-9

Cell/surface interactions on laser micro-textured titanium-coated silicon surfaces

Steven Mwenifumbo · Mingwei Li · Jianbo Chen · Aboubaker Beye · Wolé Soboyejo

Received: 20 October 2005 / Accepted: 28 February 2006

Abstract This paper examines the effects of nano-scale titanium coatings, and micro-groove/micro-grid patterns on cell/surface interactions on silicon surfaces. The nature of the cellular attachment and adhesion to the coated/uncoated micro-textured surfaces was elucidated by the visualization of the cells and relevant cytoskeletal & focal adhesion proteins through scanning electron microscopy and immunofluorescence staining. Increased cell spreading and proliferation rates are observed on surfaces with 50 nm thick Ti coatings. The micro-groove geometries have been shown to promote contact guidance, which leads to reduced scar tissue formation. In contrast, smooth surfaces result in random cell orientations and the increased possibility of scar tissue formation. Immunofluorescence cell staining experiments also reveal that the actin stress fibers are aligned along the groove dimensions, with discrete focal adhesions occurring along the ridges, within the grooves and at the ends of the cell extensions. The implications of the observed cell/surface interactions are discussed for possible applications of silicon in implantable biomedical systems.

S. Mwenifumbo · J. Chen · A. Beye · W. Soboyejo (✉)
The Princeton Materials Institute and The Department of Mechanical and Aerospace Engineering, Princeton University, Princeton, NJ 08544, USA
e-mail: soboyejo@princeton.edu

M. Li
Spectra-Physics, Inc., 1330 Terra Bella Ave., Mountain View, CA 94043, USA

A. Beye
Department of Physics, Cheikh Anta Diop University, Dakar, Senegal

1 Introduction

Over the past two decades, there have been great advances in the development of micro-electro-mechanical systems (MEMS) [1]. Most recently, MEMS structures have emerged with the potential for use in the human body. These include: micron-scale pressure sensors and MEMS drug delivery systems [2–5]. Unfortunately, there are some concerns about possible cell/surface interactions that must be addressed before such implantable systems can be fully realized. Therefore, there is a need for research that will develop surface modification methods for bioMEMS surfaces that are being developed for potential applications in biological systems.

Historically, silicon has been the material of great technological interest in MEMS. This is because of its ubiquity in the fabrication of MEMS devices. Unfortunately, immunological responses to silicon have limited its use in biological systems [6]. There are two major issues associated with the integration of silicon bioMEMS with biological tissue. The first is associated with the need for biocompatibility [6], while the second involves the adhesion and integration of cells to bioMEMS surfaces [7]. In the case of silicon biocompatibility, this can be engineered through the use of biocompatible coatings [8, 9]. Titanium, one of the few metals not shown to elicit cytotoxic reactions in the body [7, 10], serves as an ideal coating material. Previous studies have assessed the efficacy of titanium as a biocompatible coating and have indicated the minimum required nano-scale thickness [9].

In biomedical systems, surface texturing may be introduced to enhance adhesion and integration, reduce scar tissue formation, and moderate immune responses [10–19]. Several studies [11, 12, 16, 17] have indicated that the application of micro-grooves to surfaces results in the alignment of cells within grooves (contact guidance) during cell spreading and proliferation. This contact guidance has been shown to

improve wound healing and minimize scar tissue formation [16, 17]. Ordered proliferation is theorized to be the result of various phenomena; one theory suggests that contact guidance is based upon minimum free energy or path of least resistance arguments [20–22], other theories deal with the ability of cells to maintain the necessary intracellular communication [23, 24].

One such method for micro-texturing silicon surfaces is laser-ablation. Laser processing of semiconductors has been an area of intense fundamental and applied research for many years due to the technological importance of semiconductors [25]. Nano-second-laser processing of the semiconductor materials enables high heating rates in very localized regions. Consequently, numerous potential applications have emerged, ranging from laser assisted particle removal [26] to the annealing of ion-implanted semiconductor surfaces [27].

In addition, successful bioMEMS integration requires the fusion of material surfaces with the surrounding tissue. In understanding the establishment of mechanically solid interfaces, insight into the macro- and micro-scale features is necessary. In general, macro-scale features will influence the gross biomechanical stress/strain behavior between implant and tissue, while micro-scale features affect cell-implant interactions more directly [28]. Thus, an improved understanding of cell adhesion to materials with varied surface topology is required for the enhancement of cell/biomaterial integration. In prior studies [14], it has been observed that the amplitude and organization of the surface roughness will influence adhesion and proliferation. Typically, less organized surfaces with relatively high micro-roughness amplitudes will exhibit less proliferation [14].

This paper presents the results of an experimental study of cell/surface interactions on laser micro-textured titanium coated silicon surfaces that are relevant to bioMEMS structures. Silicon specimens were laser-irradiated at three different scan speeds in the horizontal and/or vertical directions of the scan field. A 50 nm thick titanium layer was applied to the specimens using electron beam vapor deposition (EBVD) to assess their biocompatibility. All analyses were performed using scanning electron microscopy (SEM), scanning white-light interferometry, and immunofluorescence microscopy. The effectiveness of the cellular attachments to the micro-textured uncoated/coated specimens is evaluated, and the implications of the results are discussed with respect to the integration of bioMEMS structures into the human body.

2 Materials and methods

2.1 Material

The single-crystalline silicon used in this study was in the form of *n*-type, phosphorus doped, (100) silicon wafers (Silicon Valley Microelectronics, San Jose, CA) with a diameter of 100 mm and a thickness of 375 microns. The nanosecond laser micro texturing was produced on rectangular specimens, approximately 6.5 mm × 16.5 mm, sectioned from the silicon wafers. After laser processing and cleaning, a 50 nm thick titanium coating was deposited on the specimens via electron-beam vapor deposition (EBVD) using a Denton DV-502A electron beam evaporator (Denton Vacuum, Moorestown, NJ). The laser processing was performed at Spectra Physics Inc., Mountain View, CA, while the EBVD was done in the clean room at the Princeton Institute of Science and Technology of Materials (PRISM) at Princeton University.

2.2 Laser processing

The silicon specimens were irradiated by nanosecond laser pulses generated by a HIPPO 355 nm diode-pumped solid-state laser (Spectra Physics, Inc., Mountain View, CA). The laser was operated at a pulse repetition frequency (PRF) of 100 kHz with pulse duration of 15 ns and an average power output of 2.5 W. A hurrySCAN 10 laser scan head (SCANLAB AG, Puchheim, Germany) with an $f = 100$ mm telecentric objective was used to focus and move the beam and the focal spot size was estimated to be approximately 8.5 microns. The specimens were mounted on a manual XYZ translational stage under the scan head. Scan speeds ranging from 300 to 800 mm/s were used to produce a series of laser ablated parallel micro-grooves along either the horizontal or vertical direction of the scan field or along both the horizontal and vertical directions. All the processing was completed in a single beam pass and the parallel grooves were produced with a 20-micron center-to-center spacing. Table 1 summarizes the processing parameters used in the production of the micro-grooved silicon specimens. The results from earlier studies [29, 30] indicated that the micro-grooves developed at a laser output of 355 nm (UV) and the processing parameters listed in Table 1 produced grooves closest to the optimal groove geometries or at osteoblasts (8 μm to 12 μm) [11, 12], which promote tissue integration. However, it is possible that different microgroove geometries would be required for "optimal" cell/surface integration of other cell types/sizes.

2.3 Surface preparation

After the laser irradiation process, the silicon specimens were cleaned in order to remove the SiO_2 deposits and loose particulates that had formed as part of the laser irradiation process. Briefly, the specimens were ultrasonically cleaned in a 1:5 aqueous solution of 48% hydrofluoric acid for 30 min at ambient temperature and pressure, removed from solution, rinsed in double distilled water (dd H_2O) and dried with N_2 gas. The silicon specimens were subsequently characterized

Table 1 Processing parameters of UV laser micro-grooved silicon

Specimen #	Pulse rate (kHz)	Groove spacing (μm)	Power (W)	Pulse duration (ns)	Scan speed (mm/s)	Spot-to-Spot spacing (μm)	fluence (J/cm^2)	Scan field direction
1	100	20	2.5	15	300	3.0	44.5	Horizontal
2	100	20	2.5	15	300	3.0	44.5	Vertical
3	100	20	2.5	15	300	3.0	44.5	Horiz./Vert.
4	100	20	2.5	15	500	5.0	44.5	Horizontal
5	100	20	2.5	15	500	5.0	44.5	Vertical
6	100	20	2.5	15	500	5.0	44.5	Horiz./Vert.
7	100	20	2.5	15	800	8.0	44.5	Horizontal
8	100	20	2.5	15	800	8.0	44.5	Vertical
9	100	20	2.5	15	800	8.0	44.5	Horiz./Vert.

using scanning electron microscopy and scanning white-light interferometry.

2.4 Surface characterization

The pre- and post-cleaning inspections of the irradiated surface regions were done with the scanning electron microscope (SEM). A Philips XL-30 field emission SEM was used to characterize the surface morphology of the laser-induced features. A detailed surface metrology of the laser-modified areas was performed with a Zygo 3-D surface profiler (Middlefield, CT) using scanning white-light interferometry. This method enables the quantification of topographical surface features with lateral and vertical accuracy in the micrometer regime.

2.5 Cell culture

To determine the efficacy for cell spreading and adhesion under physiological conditions, human osteosarcoma cells (HOS; ATCC, Manassas, VA) were incubated on the micro-textured silicon surfaces for 48 h. Prior to cell seeding, the samples were cleaned and sterilized. Each sample was ultrasonically cleaned in a solution of dd H_2O and detergent for 20 min. The titanium-coated samples were also passivated in 30% nitric acid for 15 min in addition to the cleaning procedure. All samples were then rinsed in dd H_2O, sterilized in 100% ethanol for 5 min, and dried with nitrogen gas before being placed in multi-well culture plates.

The HOS cells were cultured in 25 cm^2 flasks (Becton-Dickinson, Franklin Lakes, NJ) and maintained in an incubator at an incubation temperature of 37°C regulated with 5% CO_2, 95% air, and a saturated humidity. A Dulbecco's Modified Eagle Medium (DMEM) supplemented with 10% Fetal Bovine Serum and 1% penicillin/streptomycin/amphotericin B was used as the cell culture medium (Quality Biological, Gaithersburg, MD). At confluence, the cells were subcultured by splitting.

The cell suspension was prepared as described by the following steps: first a solution containing 0.25% trypsin in a phosphate buffer saline (PBS) solution without Ca^{++}/Mg^{++} was used to harvest the HOS cells from the culture flask. Following the addition of the trypsin solution, the flask was incubated at 37°C for 2–3 min, upon which the flask was agitated in order to release the cells from the surface. Once the cells detached from the surface of the flask, 5 ml of the serum-free DMEM were added. The contents of the flask, including the additional 5 ml of serum-free DMEM, were moved to a 15 ml conical tube and centrifuged at 3500 rpm for 3 min. The supernatant was then removed and the cells were re-suspended in serum-free DMEM. The micro-textured surfaces residing in the multi-well plates were then seeded with 50 μL of the cells suspension with an estimated cell concentration of approximately 10^5 cells/ml, as determined by a hemocytometer count. Following a two-hour attachment period, all of the media was removed from each of the wells and replaced with supplemented DMEM. The multi-well plates were then incubated in a water saturated atmosphere of 95% air - 5% CO_2 at 37°C for 48 h.

2.6 Biological fixation and SEM preparation

In order to facilitate scanning electron microscopy, the specimens were biological fixed and critically-point-dried, following the 48-h incubation period. Briefly, the specimens were removed from the multi-well plates and the cells were rinsed in 0.1 M phosphate buffer solution (PBS), fixed in a 0.1 M phosphate buffer with 3% glutaraldehyde (w/v), rinsed in a 0.1 M phosphate buffer, step-wise dehydrated in graded series of ethanol (30%, 50%, 70%, 80%, 90%, 95% and 100%) for 30 min at each concentration, critically-point-dried (Denton Vacuum DCP-1, Moorestown, NJ) with CO_2, iridium-sputter coated with a 4 nm thick coating, and examined using a Philips XL-30 Field Emission Scanning Electron Microscope at an accelerating voltage of 5 or 10 kV.

2.7 Immunofluorescence staining (IF)

After a 48-h incubation period, the specimens were stained with fluorescence-labeled antibodies to reveal cytoskeletal (actin) and focal adhesion (vinculin) proteins. The specimens were removed from the multi-well plates and the cells were then fixed for 15 min in a 3.7% formaldehyde solution. All dilutions used in the staining procedure were made up in a 'solution A' buffer (1:2000 dilution of 1 M $MgCl_2$ in PBS). The cells on the sample surfaces were then made permeable through exposure to a 0.5% Triton solution for 15 min. After the samples were rinsed in solution A, they were then exposed to the primary antiserum, containing 1:300 dilution of the primary anti-vinculin antibody in solution A plus 2.0% ovalbumin. The samples were incubated in the primary antiserum for 30 min in a humid, 37°C atmosphere. The samples were then rinsed in solution A and incubated in a secondary antiserum, containing rhodamine phalloidin in 1:500 dilution and a secondary anti-vinculin antibody in 1:600 dilution in solution A plus 2.0% ovalbumin. The samples were incubated, while exposed to the secondary antiserum for 30 min at 37°C. A small drop of FluoroGuard reagent (Bio-Rad Laboratories, Hercules, CA) was added to the seeded micro-textured specimens and coverslips were placed over the specimens. Immunofluorescence microscopy was subsequently carried out using a Nikon 50i research microscope, with an EPI-fluorescence attachment, and images were taken using a Nikon Instruments DXM 1200F color digital camera (Melville, NY).

3 Results and discussion

Laser-irradiated zones produced at three different scan speeds (300, 500, and 800 mm/s) were selected for a more detailed visual and surface metrological characterization. The zones produced during the laser ablation process consist of micro-grooves produced by irradiating in either the horizontal or vertical direction of the scan field and micro-grids formed by irradiating in both the horizontal and vertical directions of the scan field.

3.1 Scanning electron microscopy (SEM)

SEM images showing the pre-cleaned laser-ablated surfaces produced with variable scan speeds and incident beams along the horizontal and vertical directions of the scan field are presented in Fig. 1.

These regions can be qualitatively identified by their surface morphology and debris patterns. The images show two distinct, surface morphologies: micro-grooves and micro-grids. Within these two distinct morphologies, three types of surface features were generally observed: resolidification packets, striations, and groove wall deformations (Fig. 2). The splatter patterns correspond to an expulsion of material from the grooves, which result in resolidified material and the deposition of solidified silicon droplets within and around the micro-textured regions. In earlier work [29] it was determined that resolidification packet size and incidence

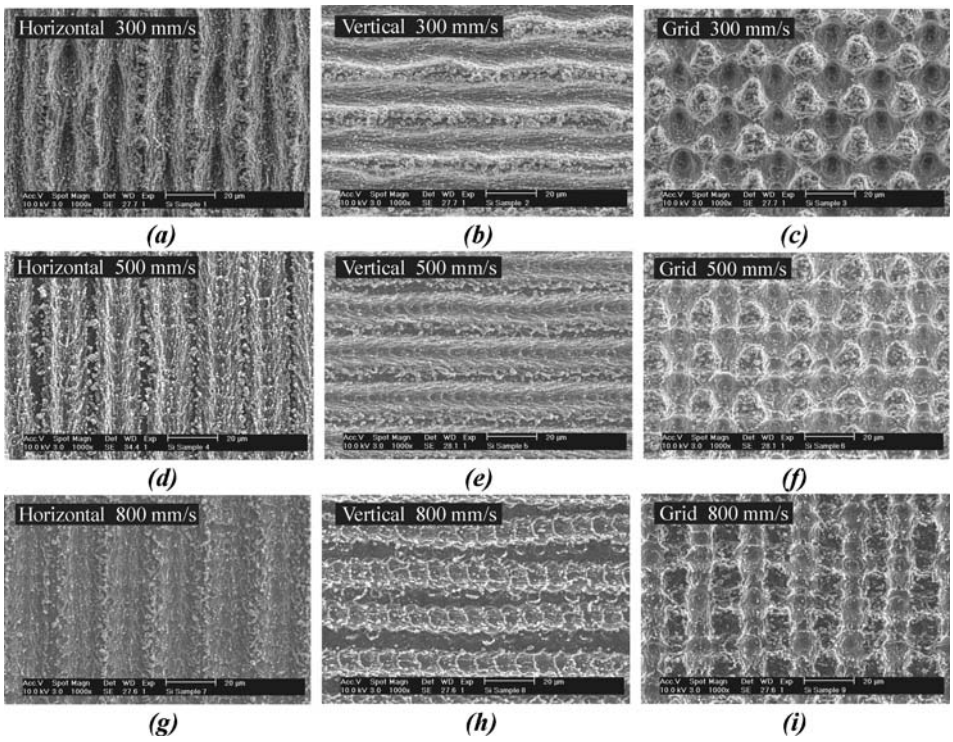

Fig. 1 SEM images of pre-cleaned UV laser-ablated grooves produced using variable scan speeds. Scan speed of 300 mm/s along the (a) horizontal, (b) vertical, and (c) horizontal and vertical directions. Scan speed of 500 mm/s along the (d) horizontal, (e) vertical, (f) and horizontal and vertical directions. Scan speed of 800 mm/s along the (g) horizontal, (h) vertical, and (i) horizontal and vertical directions

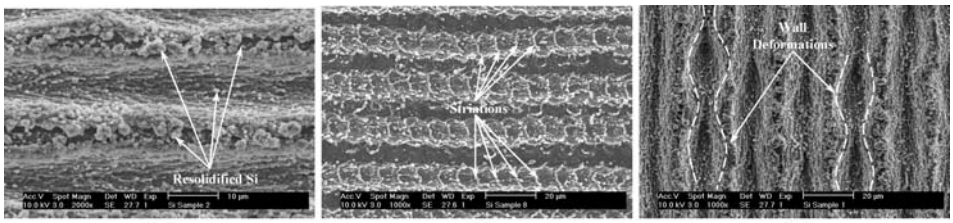

Fig. 2 Observed physical phenomenon associated with laser-irradiation of silicon specimens: (a) resolidified silicon formed during laser ablation of specimens along the vertical direction of the scan field (300 mm/s); (b) striations observed within the grooves of the silicon specimens irradiated along the vertical direction of the scan field (800 mm/s); (c) wall deformations of the 300 mm/s, horizontal direction grooves

on Ti-6Al-4V surfaces, increased by decreasing spot-to-spot spacing. In this study, a similar trend was observed.

A comparison of the distance traveled along the sample between laser pulses and the mean spacing between striations suggests that these physical marks are due to the spacing between laser pulses [30]. The absence of striations in the micro-textured surfaces produced with a scan speed of 300 mm/s is the result of more pulse overlapping and material removal at a lower speed. The motion of the scan mirrors may have contributed to the wall deformations (repeated round sections along the lengths of the grooves) observed in the parallel grooves. In addition, possible beam defocusing at certain locations of the specimen surfaces could result in an increase of the spot size and therefore an increase in the lateral size of the ablated grooves.

A slight variation between the morphology of the grooves irradiated along the vertical direction of the scan field and those irradiated in the horizontal direction was observed. Specifically, an increase appeared in the waviness of the grooves along the vertical direction (Fig. 3). Oscillation problems associated with the particular scan head used, most likely account for these variations.

The surface morphology of the silicon-irradiated samples changed with decreasing scan speed; the slower the scan speed, the larger the volume of displaced semiconductor material. This displaced material was found within and around the surface of the micro-grooves or micro-grids. Some samples in lower scan speed regimes, depicted in Fig. 4, exhibited the presence of defects within and around the micro-grooves and micro-grids, which presumably arose as a result of more thermal input from the laser at lower speeds.

The chemical/mechanical cleaning process employed to remove loose particulate and SiO_2 deposits that had formed on the laser-irradiated specimens was determined from the SEM images to be relatively effective. Figure 5 shows the typical reduction in surface particulates, for the laser micro-textured surfaces irradiated with a scan speed of 500 mm/s.

3.2 Scanning white-light interferometry

Figure 6 shows three typical Zygo 3-D surface profiles for the laser-induced features of the specimens produced using the processing parameters listed in Table 1. All the surfaces were scanned using white-light interferometry and the morphological features were analyzed using ZYGO MetroPro™ software (Middlefield, CT).

The surface metrology characterization for the laser-irradiated surfaces was performed on scan size areas of ~186 μm × 140 μm and the measurements are summarized in Table 2.

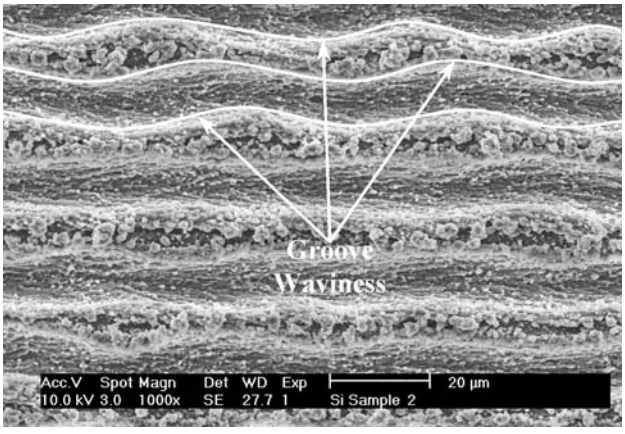

Fig. 3 Waviness variations of laser-irradiated grooves produced using a scan speed of 300 mm/s along the vertical scan field direction

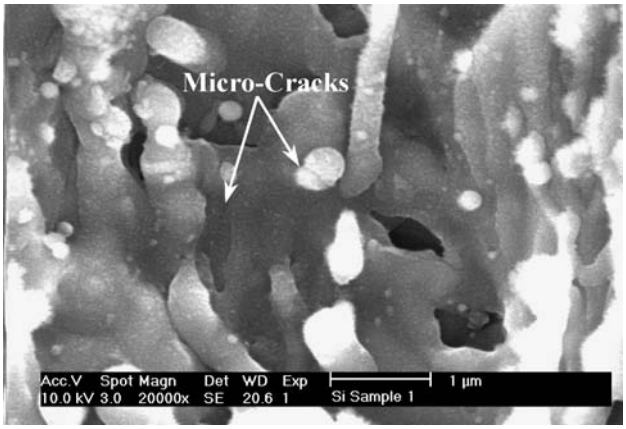

Fig. 4 SEM image of defect (micro-crack) produced within the laser-irradiated groove—scan speed of 300 mm/s along the horizontal scan field direction

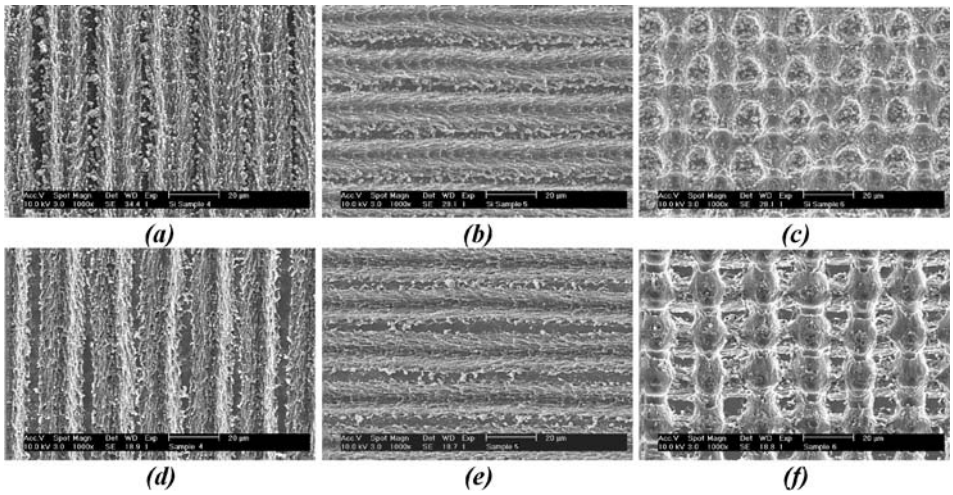

Fig. 5 SEM images of pre- and post-cleaned laser-irradiated micro-grooved specimens produced with a scan speed of 500 mm/s along the scan field directions. Pre-cleaned specimens: (a) horizontal, (b) vertical, and (c) horizontal and vertical directions. Post-cleaned specimens: (d) horizontal, (e) vertical, and (f) horizontal and vertical directions

The cross-sectional area below the original plane of the surface was found to scale approximately linearly with the scan speed. With a decrease in the scan speed (decreased spacing between laser pulses), the depth of the laser-textured features increased. In all cases, the size of the affected area was slightly larger (∼10 microns) than the focal spot size, where only the intensity of central part of the beam was significant enough to remove material. This sensitivity also means that the alignment of the focusing plane with sample surfaces is crucial. Even a small degree of defocusing leads to a rapid decrease in the beam intensity on the surface, which can either cause fluctuations in the width and depth of the features, or even reduce the intensity such that it is below the ablation threshold.

3.3 Cell spreading and morphology

The SEM images in Fig. 7 depict 48-h cultured HOS cells along with the three-dimensional structures (micro-grooves/

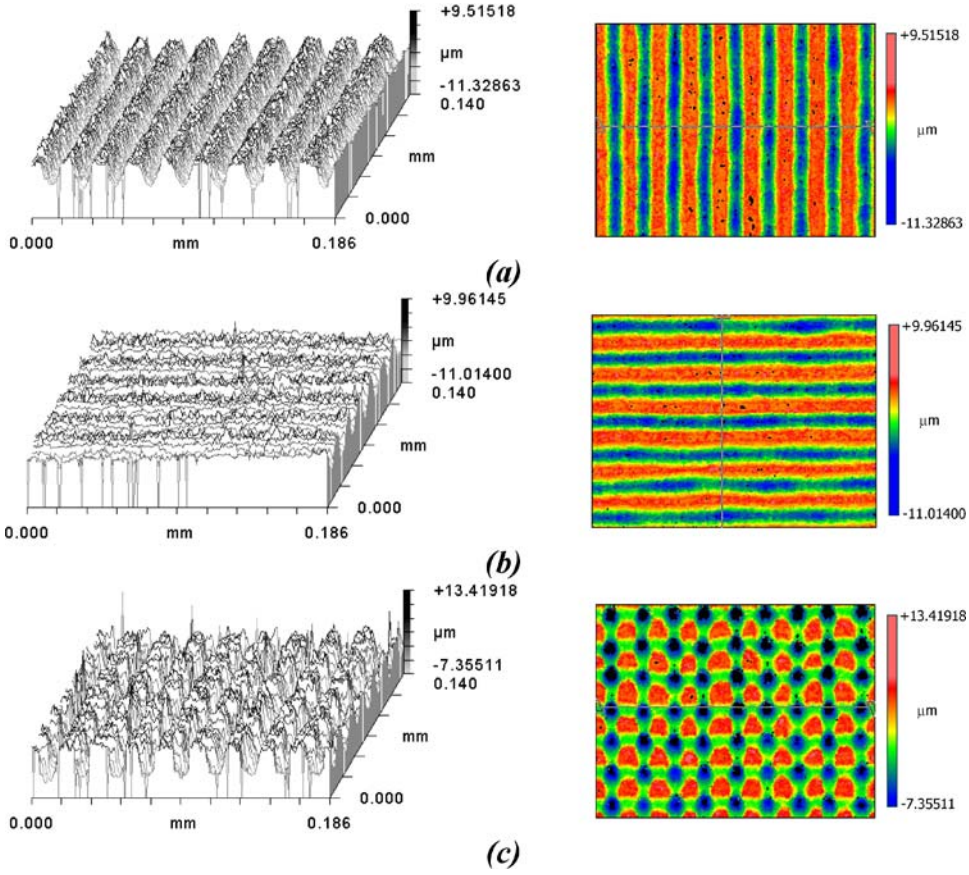

Fig. 6 3-D surface metrology images of the laser ablated micro-grooved silicon specimens with a scan speed of 500 mm/s along the (a) horizontal, (b) vertical, and (c) horizontal and vertical scan field directions

Table 2 Surface metrology of UV laser micro-textured silicon

Specimen #	Groove spacing (μm)	Groove width (μm)	Groove height (μm)	RMS surface roughness (μm)
1	20	12	11	3.95
2	20	12	11	4.04
3	20	12	14	4.46
4	20	11	9	2.47
5	20	11	9	2.45
6	20	11	12	3.53
7	20	10.5	8	1.52
8	20	10.5	7	1.46
9	20	10.5	10	3.26

micro-grids) used to investigate the response of cells to surface characteristics, patterns, and morphology.

On all the grooved specimens, the cells were oriented along the grooves (Fig. 7(a), (b), (d), (e), (g), and (h)). The cell aspect ratio (cell elongation) and the level of orientation along the groove directions decreased with decreasing groove depth and rms surface roughness. The cells cultured in the grooves processed at a scan speed of 300 mm/s were occasionally aligned in deeper grooves with minimal lateral spreading, while the cells cultured on the 800 mm/s scan speed surfaces tended to straddle the grooves more and developed a more jagged morphology (Fig. 7(g) and (h)). Although the micro-grooved surfaces played a significant role in influencing HOS cell aspect ratio and migration direction (within the grooves the cells aligned with the axis of the grooves and the movement of the HOS cells was relatively bi-directional along the axis of the grooves), the micro-grid patterns had a significantly different effect on the cells. Within the micro-grid patterns, the cells appeared to be less mobile, were found to attach to the tops of the bumps, with relatively no alignment effects, and spread minimal distances from their initial landing site.

In addition, the random nature (topology/roughness) of the micro-groove and micro-grid patterns was found to influence the spreading, proliferation, and differentiation of 48-h cultured HOS cells. Specifically, spreading and proliferation rates were found to decrease with increasing rms surface roughness, with cells cultured on the smooth surfaces having the highest spreading and proliferation rates. Figure 8 demonstrates these differences in spreading and proliferation rates at two different interfaces.

On the uncoated/coated smooth surfaces, the HOS cells were widely spread and randomly oriented after the 48-h culture period (Figs. 9(a) and (b)). The cell coverage on the smooth titanium-coated surfaces (Fig. 9(b)), was denser (near-confluence) than that of the native silicon surfaces (Fig. 9(a)). In general, all titanium-coated surfaces showed denser cell coverage, including the micro-groove and micro-grid specimens.

3.4 Immunohistochemistry

To further evaluate the behavior of cells on the different surfaces, actin and vinculin distributions were assessed to

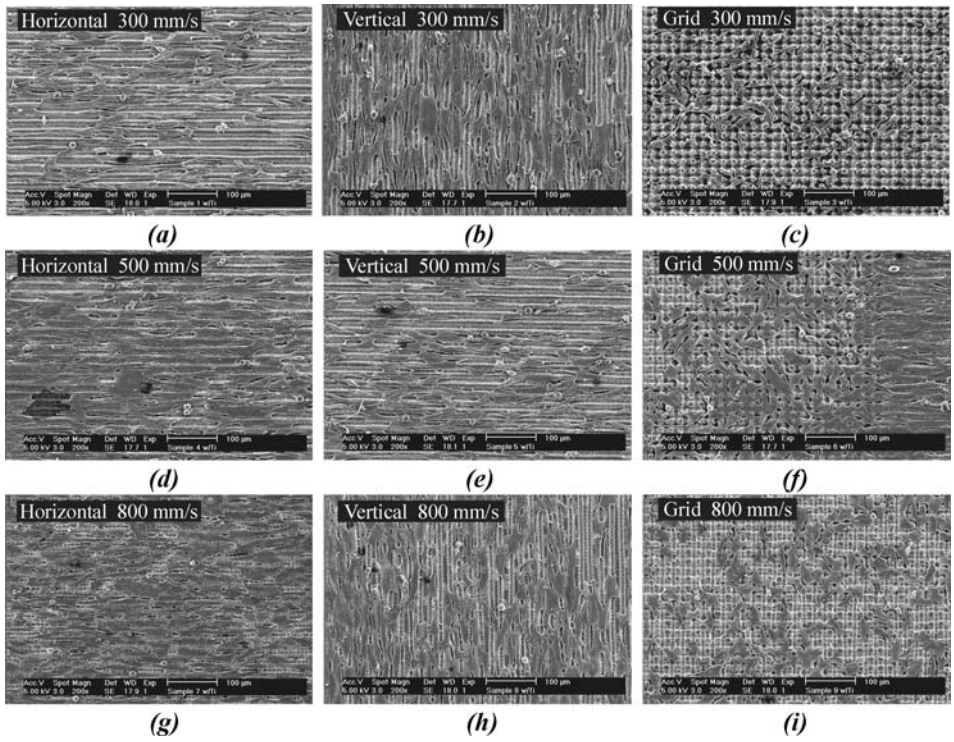

Fig. 7 Cell-surface interactions between 48-h cultured HOS cells and the laser micro-textured titanium-coated silicon surfaces. Contact guidance observed on grooved surfaces, while random cell orientations observed on micro-grid patterns. Scan speed of 300 mm/s along the (a) horizontal, (b) vertical, and (c) horizontal and vertical directions of the scan field. Scan speed of 500 mm/s along the (d) horizontal, (e) vertical, and (f) horizontal and vertical directions. Scan speed of 800 mm/s along the (g) horizontal, (h) vertical, and (i) horizontal and vertical directions

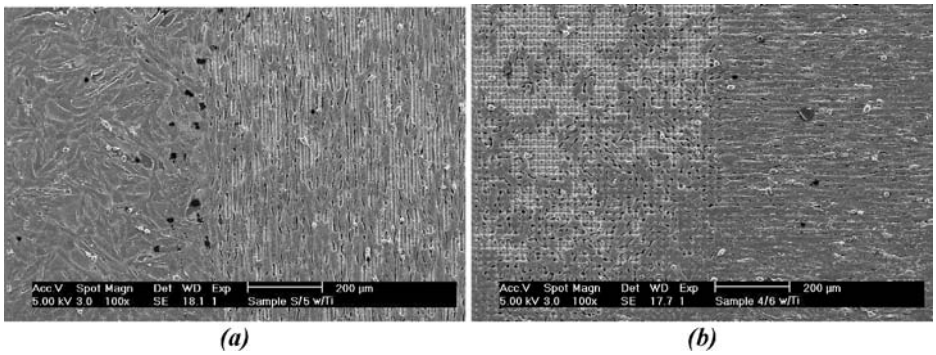

Fig. 8 SEM images of cell/surface interactions of 48-h cultured HOS cells at the (a) smooth (left) and 500 mm/s scan rate vertical groove interface (right) and the (b) 500 mm/s horizontal grooves (right) and micro-grid interface (left)

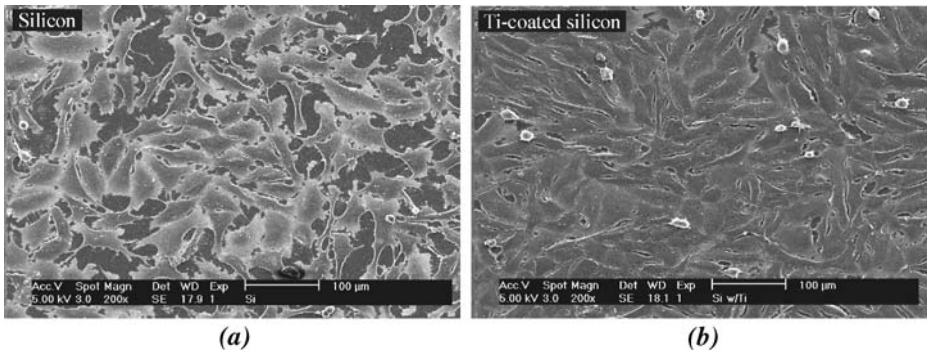

Fig. 9 Comparison of cell/surface interactions between the (a) smooth silicon and (b) smooth 50 nm thick titanium-coated silicon surfaces

describe microfilaments and focal contacts. Cytoskeletal organization and focal adhesion molecules of HOS cells cultured on silicon and titanium-coated silicon micro-textured surfaces were analyzed by immuno-fluorescence microscopy. Figures 10–12 show representative IF images of HOS cells stained for actin and vinculin after 48 h on the smooth and titanium-coated micro-textured surfaces.

As with the SEM analysis, IF staining indicated that the cells cultured on the uncoated/coated smooth surfaces were well spread. The actin microfilaments were organized in well-developed bundles with vinculin staining observed at the ends of the cell extensions. In general, the vinculin distribution occurred as distinct focal contacts localized in various regions: around cell perimeters (associated with radially distributed stress fibers) and in some cases around central areas of the cells. The majority of cells exhibited vinculin staining around the perinuclear region of the cells in addition to the discrete focal adhesions. Studies [31] suggest, that this vinculin immunoreactivity results from labeling of perinuclear regions inside the cell, and is not associated with cell-surface contacts.

The actin and vinculin distributions were somewhat different for the cells cultured on the micro-grooved and micro-grid surfaces (Fig. 11). To start, most of the cells were not as well spread as on the smooth surfaces. On the micro-grooved surfaces, the majority of cells demonstrated aligned microfilament bundles on the groove ridges, as well as in the grooves (Fig. 12(a)). The focal contacts were found predominately on the ridges, and when found within the grooves, the focal contacts were frequently located at the ends of the cells. Vinculin staining was also apparent within the cells cultured on the micro-grooved surfaces (Fig. 12(b)).

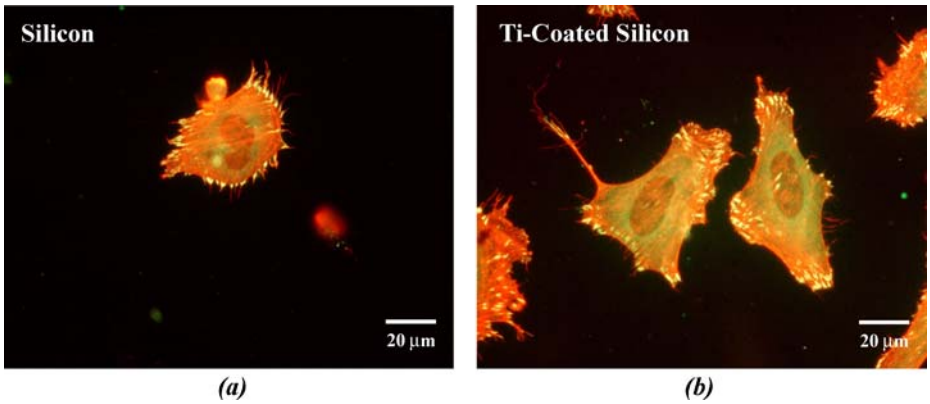

Fig. 10 IF images of HOS cells stained for actin (red) and vinculin (green) at 48 hrs. Comparison between the smooth (a) silicon and (b) 50 nm thick titanium-coated silicon surfaces

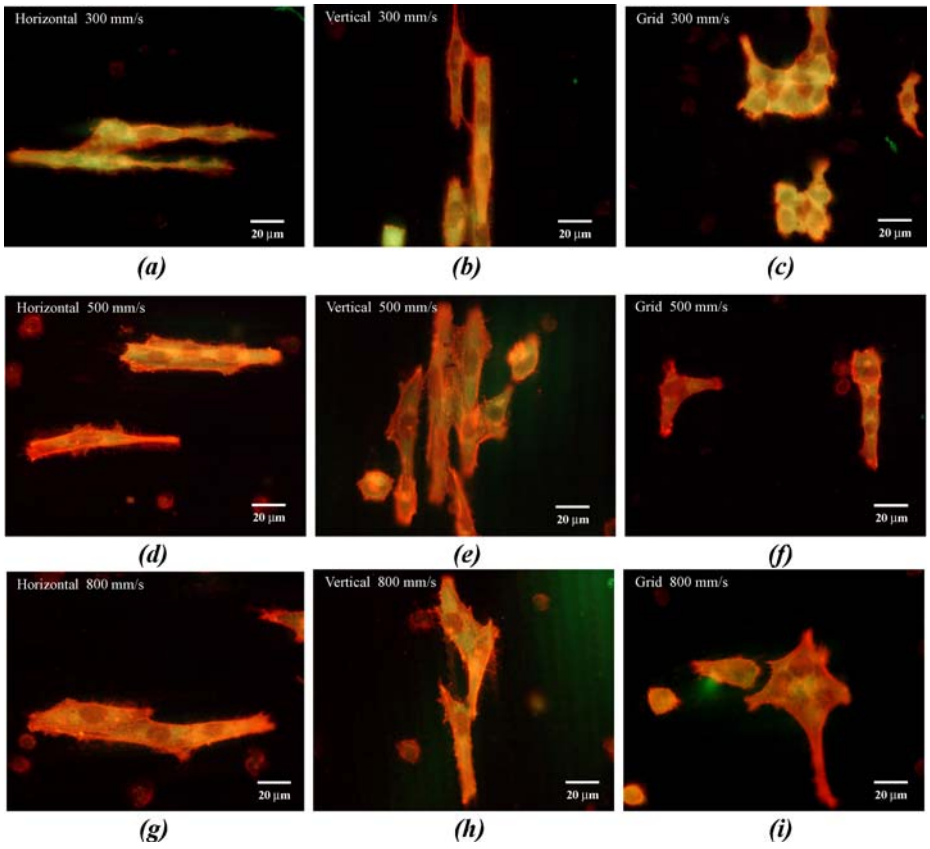

Fig. 11 HOS cells on titanium-coated silicon micro-textured surfaces fluorescently stained for actin (red) and vinculin (green) at 48 hrs. Scan speed of 300 mm/s along the (a) horizontal, (b) vertical, and (c) horizontal and vertical directions. Scan speed of 500 mm/s along the (d) horizontal, (e) vertical, and (f) horizontal and vertical directions. Scan speed of 800 mm/s along the (g) horizontal, (h) vertical, and (i) horizontal and vertical directions

The actin and vinculin distributions appeared less organized in cells growing on the micro-grid surfaces than those cultured on the micro-grooved surfaces. The micro-grid surfaces contained many thick stress fibers with a microfilament organization oriented in the direction of vertical and horizontal scan directions. Vinculin staining was observed in discrete form at the ends of some bundles, as well as in diffused form within the center of the cell.

3.5 Image analysis

The digital images of HOS cells were quantitatively analyzed for cell area, aspect ratio, and orientation angle. The imaging was done relative to vertical and horizontal axes. In the case of the microgrooved specimens, the vertical axes corresponded to the line direction of the grooves, and the horizontal direction was perpendicular to this direction. The orientations of the cells were measured using digital methods on a microcomputer. These were done on images that contained ~25.50 cells. Post-imaging analyses were carried out on ~75–100 cells per substratum using Scion Image software (Scion Corporation, Frederick, MD) for the measurements and Systat 10 software (SPSS Inc., Chicago, IL) for the statistics. A Kruskal-Wallis one-way analysis of variance by ranks was used to analyze the data because they were not normally distributed. In addition, it should be noted that the

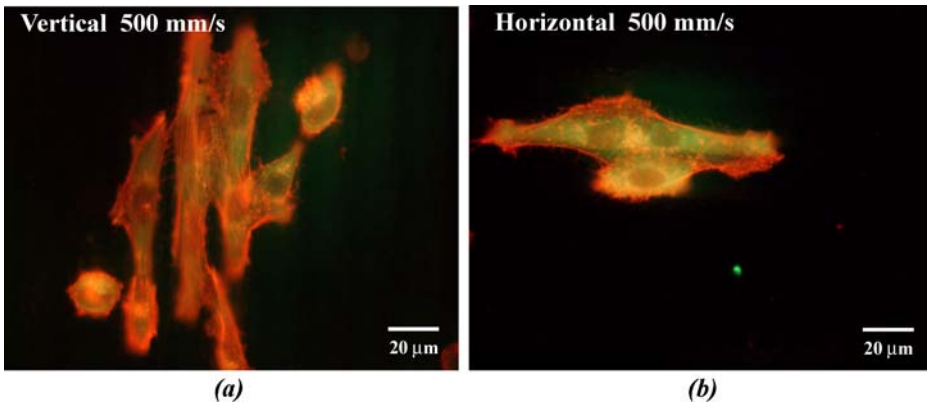

Fig. 12 HOS cells on titanium-coated silicon micro-grooved surfaces: (a) cytoskeletal arrangement (aligned actin microfilaments) and (b) diffused vinculin staining around cell nuclei

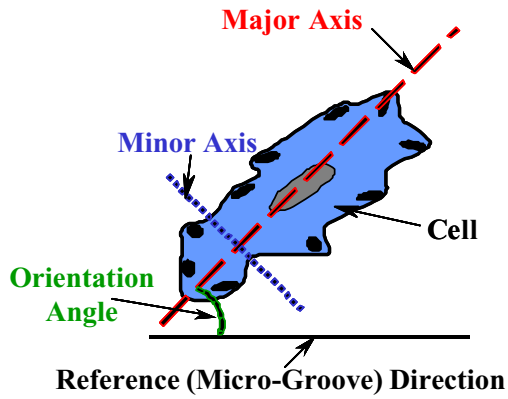

Fig. 13 Schematic showing cell orientation

smooth surfaces were used to provide a baseline comparison for cell behavior. With respect to cell orientation for the smooth surfaces, the reference direction was assumed to be parallel with the associated scan field direction comparisons. Analysis of the data confirmed the influence of surface topology on cell growth. See Figs. 14–16 and Table 3 for data on the titanium-coated micro-textured surfaces.

Comparison of the micro-textured surfaces to the smooth surfaces for all measures except cell orientation angle for the micro-grid patterns showed significant differences. For the micro-grid and horizontally scanned micro-grooved surfaces, significant differences ($p < 0.001$) were seen; cell area increased as scan speed increased (i.e. decreasing surface roughness, groove depth, and groove width). In contrast, the differences observed for cell area within the vertically scanned micro-grooved surfaces were not significant.

Analyses comparing cell aspect ratio revealed significant differences within the micro-textured groups, for the horizontally ($p < 0.001$) and vertically ($p < 0.05$) scanned micro grooved surfaces. In general, cell aspect ratio decreased with increasing scan speed (i.e. decreasing groove depth and width). However, no significant differences in cell aspect ratio were observed for the different micro-grid surfaces.

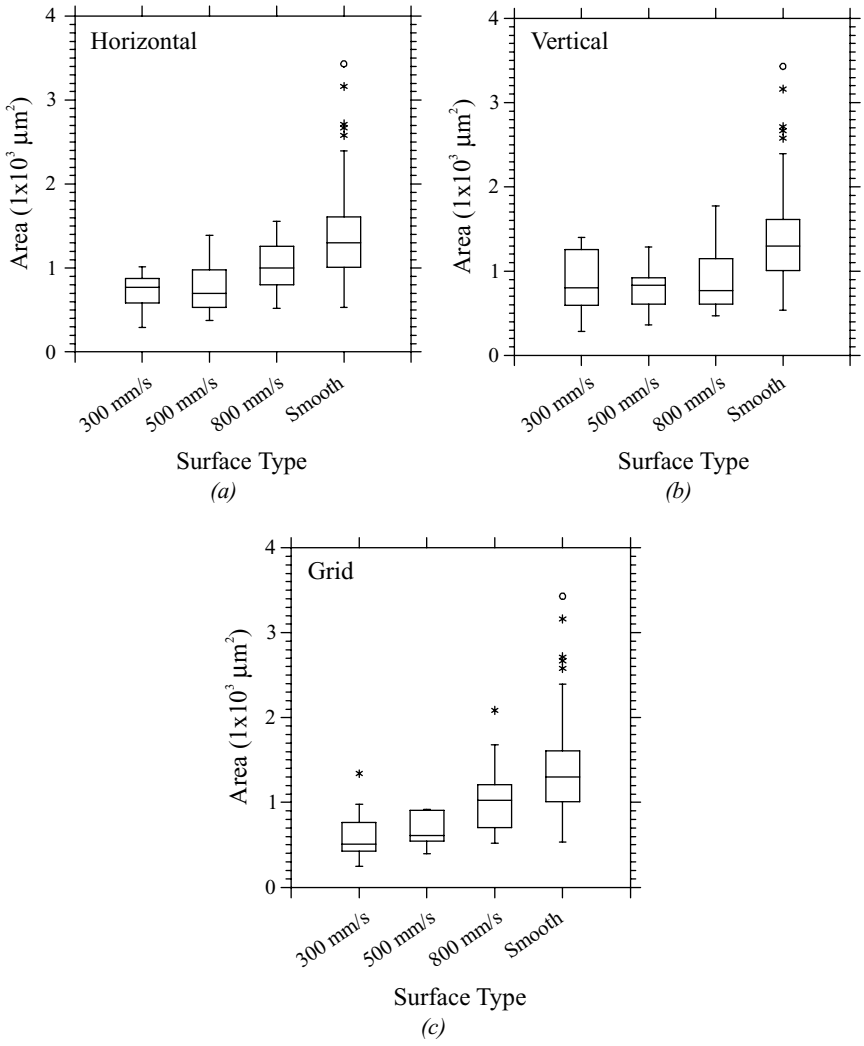

Fig. 14 Box and whisker plots of projected cell areas for 48-h HOS cells cultured on titanium-coated micro-textured surfaces: micro-grooves produced with scans in the (a) horizontal, (b) vertical, (c) and horizontal and vertical directions of the scan field

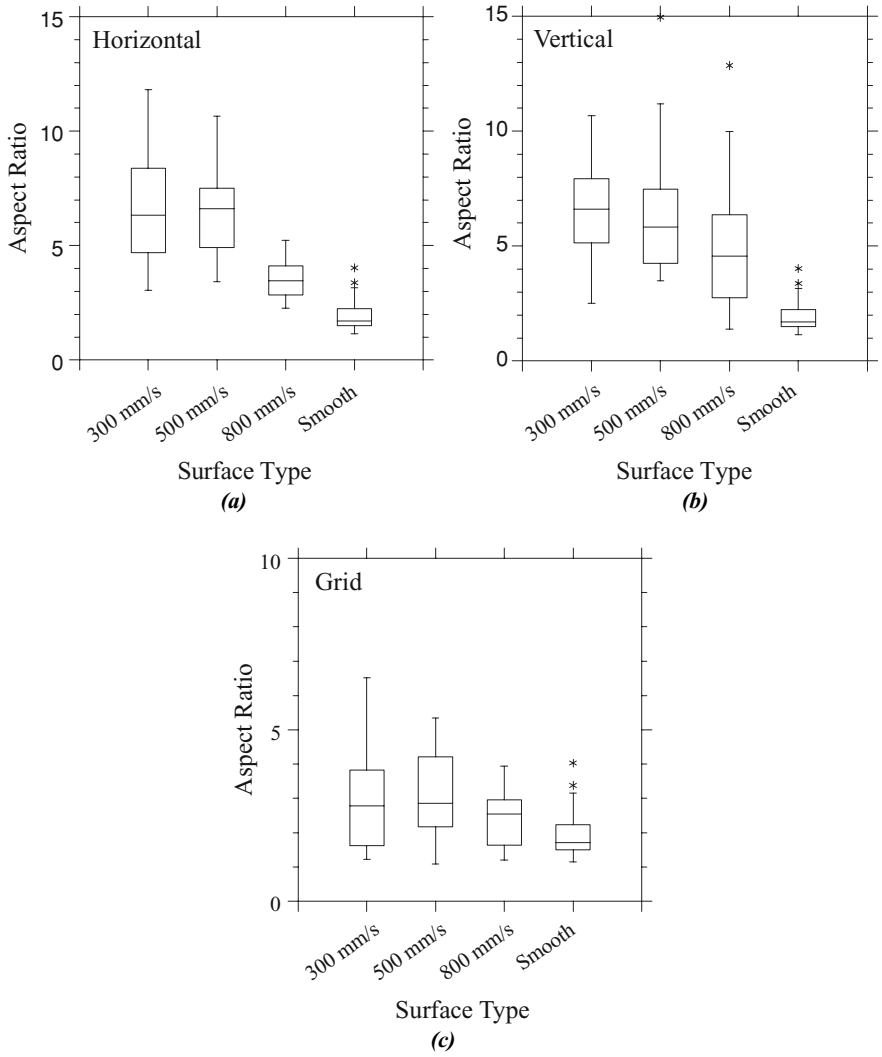

Fig. 15 Box and whisker plots of cell aspect ratio for 48-h HOS cells cultured on titanium-coated micro-textured surfaces: micro-grooves produced with scans in the (a) horizontal, (b) vertical, and (c) horizontal and vertical directions of the scan field

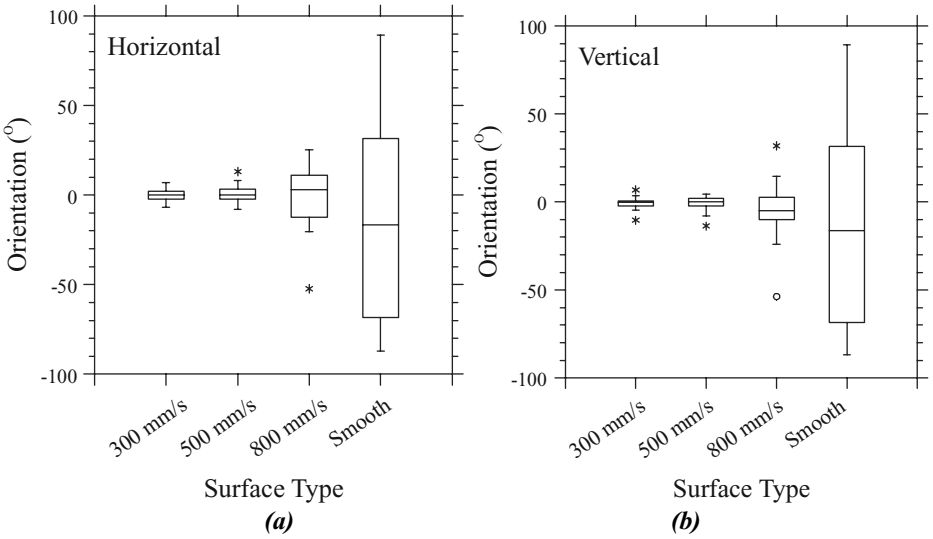

Fig. 16 Box and whisker plots of cell orientation angle for 48-h HOS cells cultured on titanium-coated micro-textured surfaces: micro-grooves produced with scans in the (a) horizontal and (b) vertical directions of the scan field

Table 3 Summary of means and standard deviations for cell area, aspect ratio, and orientation angle of HOS cells cultured on the titanium coated micro-textured surfaces

Surface type	Cell area (μm^2)	Aspect ratio	Orientation angle (°)
Smooth	1439 ± 650	1.93 ± 0.63	−10.28 ± 56.94
Section 1	713 ± 193	6.60 ± 2.29	0.01 ± 2.92
Section 2	851 ± 334	6.52 ± 2.17	−0.82 ± 3.47
Section 3	611 ± 265	2.97 ± 1.56	0.33 ± 30.76
Section 4	734 ± 286	6.34 ± 2.04	1.16 ± 4.85
Section 5	809 ± 283	6.72 ± 3.33	−1.26 ± 5.12
Section 6	690 ± 217	3.15 ± 1.56	−15.94 ± 60.91
Section 7	1043 ± 300	3.55 ± 0.78	−1.05 ± 18.11
Section 8	902 ± 382	4.93 ± 2.83	−5.37 ± 15.65
Section 9	1052 ± 418	2.48 ± 0.82	10.14 ± 58.35

Inspections of the box and whisker plots in Fig. 16 showed that the variability in cell orientation angle increased with increasing scan speed (i.e. decreasing groove depth and width). Although not shown here, analyses of the cells cultured on the micro-grid surfaces revealed cell growth was at relatively random angle orientations.

3.6 Discussion

Current attempts to develop implantable bioMEMS devices have been limited by the fact that the majority of MEMS materials are not particularly biocompatible [6]; also, the complex issues related to the adhesion and integration of implants to cells have not been fully addressed [7, 8]. This study investigated the effects of applying biocompatible coatings to silicon substrates and the effects of micro-grooves and micro-grid patterns with various depths and surface roughness on cells/surface interactions. By developing a better understanding of these issues, improvements can be made to bioMEMS technologies, reducing implant integration difficulties such as fibrous encapsulation and/or immunological reactions.

The application of a 50 nm thick titanium coating to both the smooth and micro-textured surfaces appeared to increase the biocompatibility of the silicon. The special character of titanium as a biocompatible coating has been attributed to the chemical stability and integrity of its surface oxide film [10, 32, 33]. Titanium's natural oxide film is a dense and stable anatase TiO_2 that forms to a thickness between 5 and 10 nm immediately on exposure to air [34]. It has a surface charge (isoelectric point of 5–6) that gives the passive-film a moderate charge (slightly negative) at physiological pH [32]. The oxide film's dielectric constant is comparable to water, which consequently results in Coulomb interactions of charged species that are similar to water [32]. In addition to being responsible for titanium's high corrosion resistance, the surface oxide's low overall solubility, surface charge, dielectric constant, and non-toxicity primarily account for titanium's inertness towards body fluid and integration into soft or hard tissue without major foreign body response [10].

These physio-chemical and biological properties of titanium that lead to its acceptance within the body, also influence the spreading and adhesive behavior of cells. Within this study, the titanium coating was found to have a significant effect on cell growth and spreading. Spreading, proliferation, and cell density were all found to be greater on the titanium-coated surfaces. In addition, the cells flattened out more on the titanium-coated surfaces than the native silicon surfaces. These observations confirm results obtained in a previous study by Milburn et al. [9], where a minimum coat thickness of 50 nm was determined necessary to achieve complete coverage with an EBVD layer of titanium. The pure titanium surface provides a more amiable habitat for the cells. Without complete coverage, regions of silicon emerge through the titanium layer and allow the immunological responses associated with silicon [6] to hinder cell growth. It should be mentioned, however, that further studies are required to ensure complete coverage of the laser micro-textured surfaces by the titanium layer. Unlike Milburn et al.'s smooth silicon surfaces, the morphology of laser micro-textured surfaces used in this study is rather complex. Therefore, any overhanging features may not get covered since EBVD is line of sight only.

When cells are cultured *in vitro* without the influence of external signals or cues, random cell-growth or even apoptosis may result [35]. This is largely due to the fact that important biological phenomena, such as cell growth or inhibition of growth are linked to signal transduction [36]. Within the body, tissues appear to develop by way of cues or signals that direct the growth and development of individual cells [36]. These signals may include: soluble molecules that are transported by the medium, signal molecules that reside on the surfaces of cells, physical forces, or surface morphology [37]. Aside from investigating the physio-chemical influences of titanium coatings, the influences of external signals (surface morphology) on cell development were examined through the use of micro-grooved and micro-grid surfaces. Such surfaces induce a variety of cell/surface interactions, such as contact guidance, which involves manipulating surface morphology in order to direct cell growth and movement. In numerous studies [11, 12, 16–19, 38–43], topological modifications (multiple grooves or grid patterns) have been shown to align cells on substrates and reduce inflammatory effects in soft tissue [16]. The degree of orientation depends on the cell type, surface material, and micro-texture geometry (groove, pillar/pit–width, height and depth).

No visible morphological differences were observed in cell growth within each of the three distinct coated surface morphologies (smooth, micro-grooves, and micro-grids) with the exception of the cells cultured on the 800 mm/s scan speed micro-grooves, which developed a slight jagged-polygonal morphology. Major differences did exist, however,

between the cell orientations on each of the three distinct surface morphologies. On the smooth surfaces, the cells were oriented randomly. The random nature of the observed growth may be attributed to the lack of external signals or cues to the developing cells (discussed earlier). Additionally, the surface energy associated with crystal structure alignment may have influenced the morphology of the cells, possibly accounting for the non-zero orientation of the cells on the smooth surfaces. In contrast, the cells were oriented along the grooves in the micro-grooved sections. Significant differences ($p < 0.001$) were also observed in cell spreading between the smooth and the micro-textured surfaces. The smooth surfaces exhibited larger cell spreading areas and aspect ratios of approximately 2. Scar tissue formation has been attributed to random cell growth [17], which may lead to poor tissue integration performance and impaired implant functionality. Therefore, careful consideration should be given to regions intended as sites for implant integration.

The cells cultured on the micro-grooved surfaces were found to align along the grooves and higher cell densities were observed in these areas. The variability in cell orientation angle was found to increase with increasing scan speed (decreasing surface roughness, groove depth and groove width). Specifically, within the micro-grooved surfaces, the cells cultured on the 300 mm/s and 500 mm/s scan-speed grooves demonstrated greater cell alignment than those on the 800 mm/s scan speed grooves. No appreciable differences in orientation angle variability between the 300 mm/s and 500 mm/s grooves or between the vertically and horizontally scan-field direction grooves were observed. The alignment response of the cells to the micro-grooved surfaces may be attributed to groove depth, as well as size and frequency of discontinuities. The groove depth (Table 2) and size and frequency of discontinuities (Fig. 1 - resolidification packets and striations) were found to increase with decreasing scan-speed. This is important since groove depth has been found to play an important role in the interaction between cells and micro-grooves [11, 40].

For the cultured HOS cells, a greater inhibition of groove crossing and a corresponding increase in alignment along the grooves occurred as the groove height and width increased. However, it is important to mention that the influence of height variations has been linked to cell type [38]. In this study and in [47], HOS cells lying within grooves exhibited a highly organized cytoskeletal structure and thus are more likely to be impacted by the surface morphology, suggesting that cells with a less defined structure would be less affected. In a study by Clark et al. [38], fibroblasts, epithelial cells, and neurons were all found to react strongly to the steps, while neutrophils were relatively unaffected.

The fact that cells react to discontinuities [39–43] may also explain the response of the HOS cells to the 300 and 500 mm/s scan-speed grooved surfaces. The 300 and 500 mm/s specimens (Fig. 1(a), (b), (d), and (e)) have larger and more numerous discontinuities than the 800 mm/s specimens (Fig. 1(g) and (h)). It has been postulated that discontinuities permit the condensation and the nucleation of actin [39, 40]. Within this hypothesis, contact guidance is explained by a mechanical-receptive response induced during actin polymerization. This suggests that cells will look for a balanced state where internal and external forces favor differentiation. The alignment of cells cultured on micro-grooved samples is the result of the cells being subjected to a specific configuration of forces (function of groove geometry) [40]. When the actin spikes, contained in lamellipodia at the front edges of cells, encounter a ridge (groove wall), they experience unfavorable forces that inhibit actin polymerization. In response to these unfavorable forces, actin filaments will form and elongate along the groove direction (path of least resistance) [40].

The micro-grid patterns were also found to influence cell growth and development. In all samples of the uncoated/coated silicon, the upper surfaces of the specimens were found to have the greatest influence on HOS cell proliferation, where the cells preferentially attached to the tops of the grids (pillars). The peaks/ridges of the micro-grid surfaces have the highest surface energy, possibly explaining the preferential cell attachment to these regions the observed vinculin concentrations at such high-surface energy locations. Additionally, cell growth exhibited relatively random angle orientations and no significant differences were observed for the micro-grid surfaces with respect to cell aspect ratio. However, cell area was found to increase with increasing scan speed (decreasing surface roughness, groove depth and groove width). Similar results have been found in several studies [44–46]. Craighead et al. [45] studied the behavior of both LRM55 cells and primary astrocytes on micrometer-size columns. The cells demonstrated a tendency to grow on the regions containing columns; preferentially adhering to column tops rather than the flat silicon surfaces. Green et al.'s study [44] evaluated which features, pillars (bumps) or depressions, have a greater impact on fibroblast cell proliferation. Fibroblast cells grew faster 2 and 5 μm pillared surfaces rather than the corresponding pitted surfaces. The cells were found to attach primarily to the pillar tops and it was suggested that the pillars offer more mechanical interlocking points. A study by Clark et al. [41], also found that BHK fibroblasts preferred to "ridge walk" along the sharp intersections of hill slopes rather than descending into flatter areas. Significant differences in proliferation rates were observed between the smooth surfaces and the micro-textured surfaces. In general the cells cultured on the smooth surfaces tended to reach confluence, while cell proliferation on the micro-groove and micro-grid patterns was lower. No significant differences in proliferation and attachment were observed between the 300, 500, and 800 mm/s scan-speed micro-groove surfaces, although these surfaces

did exhibit varying rms surface roughness. All micro-grid samples showed substantially lower spreading and proliferation rates compared to the micro-groove specimens even though their rms surface roughness were comparable to that of the 300 mm/s micro-groove specimens.

Examinations of the actin cytoskeletal network and focal adhesion development were performed to determine if uncoated/coated micro-textured surfaces could be exploited as interface materials for implantable bioMEMS devices. After the 48-h culture period, both the smooth and micro-grooved surfaces had well-developed organized actin microfilament bundles (stress fibers), while the micro-grid surfaces had slightly less organized actin distributions. The actin stress fibers were radial distributed on the smooth surfaces, aligned along the grooves on the micro-grooved surfaces, and predominately aligned along the vertical and horizontal scanfield directions on the micro-grid surfaces. Stained vinculin appeared throughout the cells on all the surfaces. The vinculin was almost entirely located as discrete focal adhesions on all smooth substrates (around the cell perimeter and nuclei) compared to the micro-groove and micro-grid surfaces, where it occurred along ridges, within the grooves and at the ends of the cell extensions. Vinculin was also present in diffused form throughout the cells. In general, formation of focal adhesion complexes seemed to correlate with cell spreading and that of defined actin stress fibers. It may also be affected by the increased surface stresses at the peaks and valleys of the ridges.

Despite the growing wealth of knowledge concerning physico-chemical surface modifications, a great deal is left to learn. In the present investigation, the deeper micro-grooves and the larger number of discontinuities at the micro-scale could explain the improved contact guidance and cell attachment observed with the 300 and 500 mm/s specimens compared to the 800 mm/s specimens, given that the spacing between grooves was the same for all specimens. Present experiments indicate that with controlled cell alignment and high cell density, reduced scar tissue formation and improved implant integration may be realized. The results of this study support the hypothesis that titanium biocompatible coatings coupled with UV laser surface micro-texturing, which can be easily incorporated into silicon based devices, offer useful techniques for improving the biocompatibility and tissue integration attributes of silicon-based implantable bioMEMS.

Before closing, it is important to discuss the implications of the current work for potential biomedical applications. Since titanium is a biocompatible material, it is likely that the nanoscale titanium coatings will improve the biocompatibility of silicon-based microelectronics systems and microelectro-mechanical systems (MEMS). Such improvements could greatly facilitate the potential applications of such systems in real biomedical scenarios. Furthermore, since the introduction of implants may cause scar tissue formation, the contact guidance induced by the microgrooves should significantly reduce the extent of scar tissue formation. Clearly, a combination of microgroove geometries and nanoscale coating with titanium should provide the desired combination of improved biocompatibility and reduced scar tissue formation required for actual applications. These require *in-vivo* studies (of such grooved and coated surfaces) which are beyond the scope of the current work.

4 Conclusions

The morphology, attachment, and proliferation of human osteosarcoma cells on laser-irradiated titanium coated/uncoated silicon surfaces with different micro-groove and micro-grid patterns were investigated and a summary of the salient conclusions is presented below.

1. Improved biocompatibility of the silicon surfaces was achieved by means of 50 nm-thick titanium coatings, as seen through higher HOS cell spreading and proliferation rates.
2. Enhanced orientation was observed on the titanium-coated silicon micro-grooved surfaces irradiated at scan speeds of 300 and 500 mm/s, with a micro-roughness characterized by higher rms surface roughness. It appears that cultured human osteosarcoma spread less on rougher textured surfaces than they do on "smoother" surfaces. Also, the rough groove, geometrie with depths of $\sim$9–11 μm resulted in the best combination of contact guidance and cell integration.
3. Co-localization of actin and vinculin showed that the actin formed numerous stress fibers throughout the cells, which terminated at the cell periphery and that the vinculin-containing adhesion plaques were situated at the terminal ends of the actin stress fibers.
4. Within the micro-grooved surfaces, the actin stress fibers aligned along the grooves and discrete focal adhesions occurred along ridges, within the grooves and at the ends of the cell extensions. This suggests controlled cell alignment and adhesion may be tailored to reduce scar-tissue formation and improve implant integration in microelectronics systems and bioMEMS structures that are fabricated from silicon. *In-vivo* studies are needed to further explore the potential of such silicon implants for improved integration with biological tissue and organs.

Acknowledgments The authors acknowledge support for this work provided by the National Science Foundation (Grand No. DMR-0231418) and Spectra Physics, Inc. The authors are grateful to the Program Manager, Dr. Carmen Huber, for her encouragement and support.

References

1. J. W. GARDNER, V. K. VARADAN and O. O. AWADELKARIM, "Microsensors, MEMS, and Smart Devices" (Wiley, New York, 2002).
2. B. ZIAIE and K. NAJAFI, *Biomed. Micr.* **3**(4) (2001) 285.
3. D. LIEPMANN, in Proceedings of The 3rd Korean MEMS Conference (Seoul, 2001) p. 13.
4. BABAK ZIAIE X. CAO, S. LAI and L. LEE, *Biomed. Micr.* **3**(2) (2001) 109.
5. Z. STRONG, A. WANG and C. MCCONAGHY, *Biomed. Microdevices* **4**(2) (2002) 97.
6. G. VOSKERICIAN, M. S. SHIVE, R. S. SHAWGO, H. VON RECUM, J. M. ANDERSON, M. J. CIMA and R. LANGER, *Biomater.* **24** (2003) 1959.
7. B. D. RATNER, A. S. HOFFMAN, F. J. SCHOEN and J. E. LEMONS, "Biomaterials Science: An Introduction to Materials in Medicine" (Academic Press, San Diego, 1996).
8. Y. HANEIN, Y. V. PAN, B. D. RATNER, D. DENTON and K. F. BÖHRINGER, *Sens. Act. B: Chem.* **81**(1) (2001) 49.
9. C. MILBURN, S. MWENIFUMBO, E. KUNG and W. O. SOBOYEJO, Effects of biocompatible nano-scale titanium coatings on cell spreading and adhesion to biomems structures, *to be submitted*.
10. D. M. BRUNETTE, "Titanium in Medicine: Material Science, Surface Science, Engineering, Biological Responses and Medical Applications" (Springer-Verlag, New York, 2001).
11. W. O. SOBOYEJO, B. NEMETSKI, S. ALLAMEH, N. MARCANTONIO, C. MERCER and J. RICCI, *J. Biomed. Mater. Res.* **62** (2002) 56.
12. W. O. SOBOYEJO, C. MERCER, S. ALLAMEH, B. NEMETSKI, N. MARCANTONIO and J. L. RICCI, *Key Eng. Mater.* **198–199** (2001) 203.
13. K. ANSELME, P. LINEZ, M. BIGERELLE, D. LE MAGUER, A. LE MAGUER, P. HARDOUIN, H. F. HILDEBRAND, A. IOST and J. M. LEROY, *Biomater.* **21** (2000) 1567.
14. K. ANSELME, M. BIGERELLE, B. NOEL, E. DUFRESNE, D. JUDAS, A. IOST and P. HARDOUIN *Biomed. Mater. Res.* **49** (2000) 155.
15. K. ANSELME, B. NOEL and P. HARDOUN, *J. Mater. Sci.: Mater. Med.* **10** (1999) 815.
16. J. L. RICCI and H. ALEXANDER, *Key Eng. Mater.* **198–199** (2001) 179.
17. J. L. RICCI, J. CHARVET, S. R. FRENKEL, R. CHANG, P. NADKARNI, J. TURNER and H. ALEXANDER, "Bone response to laser microtextured surfaces", Bone Engineering, edited by J. E. Davies, (Em^2 Inc., Toronto, 2000) p. 1.
18. J. H-C WANG, E. S. GROOD, J. FLORER and R. WENSTRUP, *J. Biomech.* **33** (2000) 729.
19. J. H.-C. WANG and E.S. GROOD, *Connective Tissue Res.* **41** (2000) 29.
20. K. D. CHESMAL and J. BLACK, *J. Biomed. Mater. Res.* **29** (1995) 1089.
21. K. D. CHESMAL, C. C. CLARK, C. T. BRIGHTON and J. BLACK, *J. Biomed. Mater. Res.* **29** (1995) 1101.
22. E. DEN BRABER, J. DE RUIJTER, H. SMITS, L. GINSEL, A. F. VON RECUM and J. A. JANSEN, *J. Biomed. Mater. Res.* **29** (1995) 511.
23. J. L. RICCI, J. CHARVET and R. CHANG, in Proceedings of *20th Annual Meeting of the Society for Biomaterials* (Boston, 1994) p. 401.
24. P. CLARK, D. COLES and M. PECKHAM, *Exp. Cell Res.* **230** (1997) 275.
25. R. F. WOOD, C. W. WHITE and R. T. YOUNG, "Semiconductors and Semimetals 23" (Academic, Orlando, 1984).
26. M. MOSBACHER, H. J. MUNZER, M. BERTSCH, V. DOBLER, N. CHAOUI, J. SIEGEL, R. OLTRA, D. BAUERLE, J. BONEBERG and P. LEIDERER, "Laser assisted particle removal from silicon wafers", Particles on Surfaces: Detection, Adhesion and Removal 7, (VSP International Science Publisher, Netherlands, 2002), p. 275.
27. A. G. CULLIS, *Reports Prog. Phys* **48** (1985) 1155.
28. S. VERCAIGNE, J. WOLKE, I. NAERT and J. JANSEN, *J. Biomed. Mater. Res.* **41** (1998) 41.
29. M. LI, N. MORRIS, S. MWENIFUMBO, M. KEIRSTEAD and W. SOBOYEJO, in Proceedings of SPIE *4830* (Osaka, 2002) 206.
30. S. MWENIFUMBO, N. D. MORRIS, M. LI and W. O. SOBOYEJO, "Surface Engineering in Materials Science II" (San Diego, 2003) p. 141.
31. A. M. P. TURNER, N. DOWELL, S. W. P. TURNER, L. KAM, M. ISAACSON, J. N. TURNER, H. G. CRAIGHEAD and W. SHAIN, *J. Biomed. Mater. Res.* **51** (2000) 430.
32. N. D. SPENCER and M. TEXTOR, Surface Modification, Surface Analysis and Biomaterials. Materials in Medicine, edited by MD, Speidel and P Uggowitzer, (ETHZ, 1998).
33. B. FENG, J. Y. CHEN, S. K. QI, L. HE, J. Z. ZHAO and X. D. ZHANG, *J. Mater. Sci.: Mater. Med.* **13** (2002) 457.
34. B. FENG, J. WENG, B. C. YANG, J. Y. CHEN, J. Z. ZHAO, L. HE, S. K. QI and X. D. ZHANG *Mater. Character.*, **49** (2003) 129.
35. M. E. CHICUREL, C. S. CHEN and D. E. INGBER, *Curr. Opin. Cell Biol.* **10** (1998) 232.
36. E. RUOSLAHTI and B. OBRINK, *Exp. Cell Res.* **227** (1996) 1.
37. K. ANSELME, *Biomater.* **21** (2000) 667.
38. P. CLARK, P. CONNOLLY, A. CURTIS, J. DOW and C. WILKINSON, *Development* **99** (1987) 439.
39. A. CURTIS and C. WILKINSON, *Biomater.* **18** (1997) 1573–1583.
40. X. F. WALBOOMERS, W. MONAGHAN, A. CURTIS and J. A. JANSEN, *J. Biomed. Mater. Res.* **46** (1999) 212.
41. P. CLARK, P. CONNOLLY, A. CURTIS, J. DOW and C. WILKINSON, *Development* **108** (1990) 635.
42. A. CURTIS and P. CLARK, *CRC Rev. Biocomp.* **5** (1990) 343.
43. J. MEYLE, K. GUTLIG and W. NISCH, *J. Biomed. Mater. Res.* **29** (1995) 81.
44. A. GREEN, J. JANSEN, J. VAN DER WAERDEN and A. VON RECUM, *J. Biomed. Mater. Res.* **28** (1994) 647.
45. H. G. CRAIGHEAD, S. W. TURNER, R. C. DAVIS, C. JAMES, A. M. PEREZ, P. M. ST. JOHN and M.S. ISAACSON. *J. Biomed. Dev.* **1**(1) (1998) 49.
46. J. A. T. DOW, P. CLARK, P. CONNOLLY, A. S. G. CURTIS and C. D. W. WILKINSON, *J. Cell. Sci. Suppl.* **8** (1987) 55.
47. S. MWENIFUMBO, Cell/surface interactions and adhesion on biomedical and biomems surfaces: effects of laser micro-texturing and titanium coatings, A thesis of Princeton University (2004) p. 41.
48. D. WANG, K. CHRISTENSEN, K. CHAWLA, G. XIAO, P. H. KREBSBACH and R. T. FRANCESCHI, *J. Bone. Miner. Res.* **14**(6) (1999) 893.